European Polymer Journal 208 (2024) 112849

Contents lists available at ScienceDirect

European Polymer Journal

journal homepage: www.elsevier.com/locate/europolj

Review

Polymeric precision doping as an emerging technology for the downscaling of microelectronic devices: State of the art

Riccardo Chiarcos [a], Michele Laus [a,*], Michele Perego [b]

[a] Dipartimento di Scienze e Innovazione Tecnologica (DISIT), Università del Piemonte Orientale (UPO), Viale T. Michel 11, 15121 Alessandria, Italy
[b] CNR-IMM Unit of Agrate Brianza, Via C. Olivetti 2, 20864 Agrate Brianza, Italy

ARTICLE INFO

Keywords:
Doping
Semiconductor
Surface functionalization
Grafting to reaction
Polymer brush
Polypetoid

ABSTRACT

The pressing trend towards downscaling of microelectronic devices constantly requires updated technologies capable of precise control of dopant atom dose in semiconductive substrates. An emerging approach based on the grafting reaction of functionalized dopant polymers, named Polymeric Precision Doping (PPD), has proven to be a promising candidate in this direction. Precisely, the molecular weight of the dopant polymers was demonstrated to be an effective key for the precise control of doping process. In this review, the overall PPD process is described paying particular focus on the physico-chemical mechanism underlying the grafting reaction of dopant polymers. Furthermore, all the already reported dopant polymers are described, moving from first generation systems characterized by narrow distributions of molecular weights to the most recent developments of totally monodisperse bioinspired polymers.

1. Introduction

The introduction of substitutional impurities into the semiconductor lattice, generally referred to as *doping*, provides the control of the conductive properties of silicon and represents the basis of the entire semiconductor industry [1]. By properly controlling the local doping of semiconductors, junctions are formed and combined to create microelectronic devices. An inexorable trend towards the dimensional reduction of microelectronic devices has been assessed for several decades and empirically described by the well-known Moore's law [2]. Enhanced performances associated with low power consumption have made such miniaturization ever desirable over the years until, in 2012, the physical limit of the process was reached for planar transistors (MOSFET) [3,4]. Three-dimensional devices, such as FinFET transistors, were therefore rapidly implemented in order to take another step in path of miniaturization [6], achieving the extraordinary results of 5 nm transistors. A further size reduction to 3 nm transistors is currently being attempted by using new types of 3D designs [6]. Furthermore, this trend towards nanostructured devices is not limited to the transistor industry, but is also relevant, for example, in the solar cell field. In fact, solar cells designed with nanostructured surfaces are more efficient in collecting light [7].

An inevitable drawback of microelectronic devices featuring characteristic dimensions of few nanometers is that the assumption of homogeneously distributed dopant atoms becomes no longer valid [8,9,10,11,12]. In fact, in such small volume of silicon only a few dopant atoms are contained and statistical fluctuations in concentration could generate unreproducible performances in replicas of the same device. Technologies that allow to locate single dopant atoms in well-defined positions are currently available but they are still extremely time consuming. Processes such as *Single Ion Implantation (SII)* [8] or *Scanning Tunneling Microscopy (STM)* [13] provides the total control of dopant atoms required by frontier researches, such as solid-state quantum computers [14], but they are too slow for large scale applications. On the other hand, doping processes classically used in microelectronic industry lack necessary characteristics to still be valid in the new era of nano-devices. In Table 1, the most commonly used doping technologies are summarized with their respective technical specifications [7].

Ion Implantation, for example, which is based on accelerated dopant ions collimated and directly injected in silicon, allows excellent control of both position and quantity of dopant atoms. In a very recent paper, ultra-low energy ion implantation has been combined with mesoporous polymer templates obtained by block copolymer self-assembly to generate periodic arrays of p-n junctions at the nanoscale [15]. Unfortunately, ion implantation is not compatible with 3D structures due to its directionality. Furthermore, energetic ions are responsible for defect

* Corresponding author.
E-mail addresses: riccardo.chiarcos@uniupo.it (R. Chiarcos), michele.laus@uniupo.it (M. Laus), michele.perego@mdm.imm.cnr.it (M. Perego).

https://doi.org/10.1016/j.eurpolymj.2024.112849
Received 12 November 2023; Received in revised form 31 January 2024; Accepted 7 February 2024
Available online 14 February 2024
0014-3057/© 2024 The Author(s). Published by Elsevier Ltd. This is an open access article under the CC BY-NC-ND license (http://creativecommons.org/licenses/by-nc-nd/4.0/).

Table 1
Main silicon doping techniques with specified if annealing-driven diffusion step and vacuum are required. The obtainable depths of dopant atoms are also reported [7].

Doping technology	Annealing at high temperatures required for dopant atoms diffusion	Vacuum required	Achievable diffusion depth (nm)
Ion Implantation	No	Yes	< 1000
Atmospheric Pressure CVD	Yes	No	100–3000
Plasma Enhanced CVD	Yes	Yes	100–3000
Solid Source Dotation	Yes	No	100–3000
Spin-On Dopant	Yes	No	10–3000
Monolayer Doping	Yes	No	< 100

formation in the silicon crystal lattice, making necessary high temperature thermal treatments to remove such defects and activate dopant atoms [1,7,16].

On the contrary, milder doping techniques, such as *Chemical Vapor Deposition (CVD)*, definitely lack dose control and homogeneity of dopant atoms. Different types of CVD technique are currently available, such as *atmospheric pressure CVD* [17,18] or *plasma-enhanced CVD* [19], and all of these produce dopant oxide layers over silicon with a subsequent drive-in carried out at temperatures higher than 1000 °C. Such high temperature processes allow the dopant atoms to diffuse in silicon at depths ranging from 100 to 3000 nm as a function of the diffusion time [7]. Similarly, in *Solid Source Dotation* processes, dopant layers are grown on silicon by evaporating dopant species from solid sources, such as boron nitride wafers for boron doping [20], and subsequently injected into the silicon substrate by high temperature annealing.

Alternatively, dopant containing layers are provided by *Spin-On Dopant (SOD)* technology [21]. Such layers are obtained by spin-coating solutions generally containing silica or inorganic polymers and dopant atoms, typically boron (B) or phosphorus (P). After a short thermal annealing step conducted at low temperatures to evaporate the solvent and vitrify the dopant layer, the temperature is increased up to 1000 °C to promote the diffusion of dopant atoms. Finally, the glassy layer is generally removed by hydrofluoric acid treatment. The main advantage of SOD technology is that the spin-coating step leading to the dopant layer is accomplished in less than 30 s with no vacuum requirement. Interestingly, ultra-shallow junctions are obtained by diffusing dopant atoms just 10–15 nm deep in silicon by *Rapid Thermal Annealing (RTA)* process [22].

Recently, organic polymers with dopant containing moieties were introduced in SOD technology as a viable alternative to classical systems, significantly improving the control over the dopant dose and the homogeneity of the dopant atoms distribution over the substrate. In this specific system, the dopant layer is burnt away during the high temperature annealing step required to promote the injection of dopant atoms. For example, poly(vinylboronic acid pinacol ester) and poly (diethyl vinylphosphonate) polymers have been proposed and tested as the sources of B and P, respectively [23,24]. B and P concentrations about $\sim 10^{19}$ atoms/cm^3 were obtained, with depth distributions that are functions of both time and temperature of the anneling step. Additionally, several authors also reported that block-copolymer *self-assembly* can be exploited as an alternative to conventional lithography to localize dopant atoms by using copolymers having one block that contains dopant moieties [25,26]. The main drawback of SOD technology based on organic polymers is the possible silicon contamination by unwanted impurities, such as carbon, which are responsible for partial deactivation of dopant atoms [27].

A decisive advance in the search of a precision-doping technique that can be implemented on an industrial scale was carried out in 2008 with the introduction of the so-called *Monolayer Doping (MLD)* technology [28]. This approach is based on the chemical reaction of molecules containing a dopant atom with the silicon surface in order to obtain a self-assembled monolayer. In this way, the processable number of dopant atoms is both numerically controlled by the steric hindrance of the molecule and homogeneously distributed over the silicon surface. Furthermore, homogeneous coverages are obtained even in the case of patterned surfaces with 3D devices. A schematic picture of the MLD process as well as the chemical structures of some of the employed molecules are reported in Fig. 1 **(a)**. Such self-assembled monolayer is consequently covered by a $\sim$ 50 nm thick capping layer of silicon oxide (SiO_2) and dopant atoms are diffused in silicon by conventional RTA processes conducted for different annealing times and temperatures. *Secondary-Ion Mass Spectrometry (SIMS)* measurements were carried out to characterize the dopant atom concentration in silicon as a function of the depth from the Si/SiO_2 interface. In Fig. 1 **(b)** the boron doping profiles for the samples annealed for 5 s at 950 and 1000 °C are reported as a typical example. Both samples are characterized by boron distributions that are fully compatible with a finite source model: concentrations of $\sim 5 \times 10^{20}$ atoms/cm^3 are found close to the interface then decreasing to $\sim 10^{17}$ atoms/cm^3 at the depths of 18 and 43 nm for the samples annealed at 950 and 1000 °C, respectively. Highly doped regions with very reduced depths can then be obtained by opportunely tuning the annealing temperature and the time. Interestingly, the number of active B atoms was estimated by sheet resistance measurements around 1.7×10^{14} atoms/cm^2 (1.7 atoms/nm^2) whereas the complete coverage of the surface by the monolayer was calculated to carry about 4.9×10^{14} atoms/cm^2. Accordingly, only 34 % of B atoms were then correctly diffused in silicon and this fact was attributed to a B loss occurring in the upper SiO_2 layer. Conversely in the case of P doping experiments, $\sim$ 95 % of the P atoms contained in the monolayer, i.e. $\sim 7.9 \times 10^{14}$ atoms/cm^2 results diffused in the silicon substrate and activated during the thermal treatment. This result was explained by considering that P diffusivity in SiO_2 is two orders of magnitude lower compared to the one of B atoms(3.2×10^{-18} cm^2/s vs 1.4×10^{-16} cm^2/s) [29], making phosphorus less likely to diffuse in the upper oxide layer.

The suitability of the MLD technique for producing ultra-shallow junctions was then demonstrated by diffusing P atoms at a depth of $\sim$ 2 nm by spike-annealing at temperatures higher than 900 °C [30]. In this case, an activation efficiency (η) of $\sim$ 70 % was obtained for the P atoms, meaning that only this percentage of the diffused atoms is electrically active. The inactivity of the remaining 30 % was attributed to the interstitial nature of these impurities, which are not included in the silicon crystal lattice and then remain excluded from the possibility of acting as electron donors. The presence of such interstitial atoms seems to be promoted by the spike-annealing treatment. A more precise control of the dopant dose in the self-assembled monolayer was then obtained through self-assembled monolayer containing both dopant and neutral molecules [28]. Accordingly, Ye et al. reported a considerable control over the P dose by changing the molar ratio between diethyl vinylphosphonate, which is the dopant molecule, and 1-undecene, the neutral species [31]. The drawback of this approach is clearly the loss of homogeneity in the monolayer due to the random location of dopant and neutral species. Interestingly a localized doping process was instead implemented by combining the MLD technique with the use of lithographic masks [32]. This approach allows to combine the accurate control of dopant dose provided by MLD with the possibility to locate dopant atoms in well-defined regions of the substrate by conventional lithography. Finally, MLD technique was also extended to semiconductive materials other than silicon such as germanium by proper design of the dopant containing molecules [33].

Some comments regarding the chemistry underlying the MLD technique are now needed. A large number of the described dopant molecules are bonded to the silicon substrate through the reaction between a vinyl group and the SiH groups present on the silicon surface [28,31,34]. Such reaction is generally named as *hydrosilylation* [35] and is represented in Fig. 2 **(a)** in case the reactive molecule is allylboronic acid

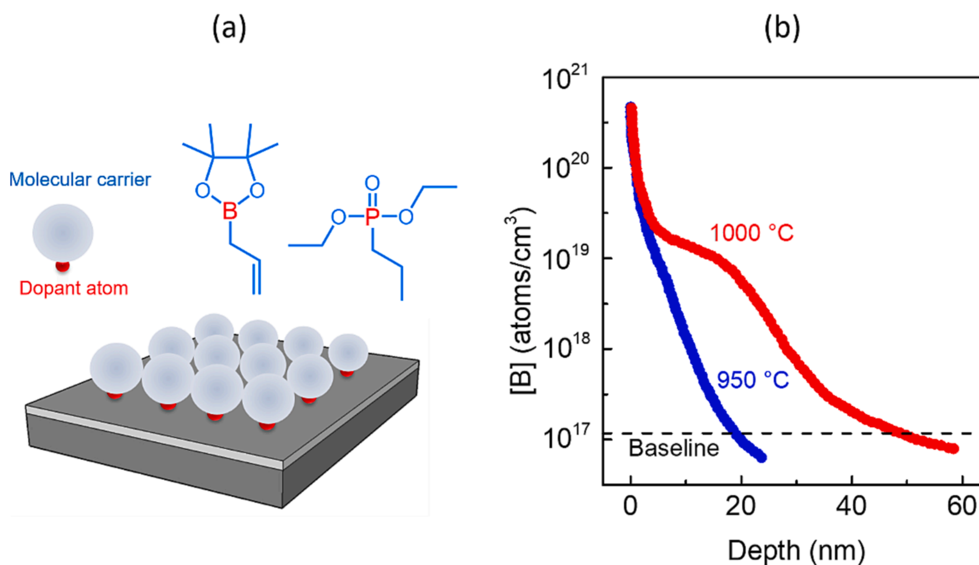

Fig. 1. (a) Monolayer doping (MLD) technique representation. The chemical structures of the dopant molecules are also included [28]. (b) Calibrated depth profiles showing B concentration [B] as a function of the depth from the interface Si/SiO_2 for the samples annealed at 950 and 1000 °C for 5 s.

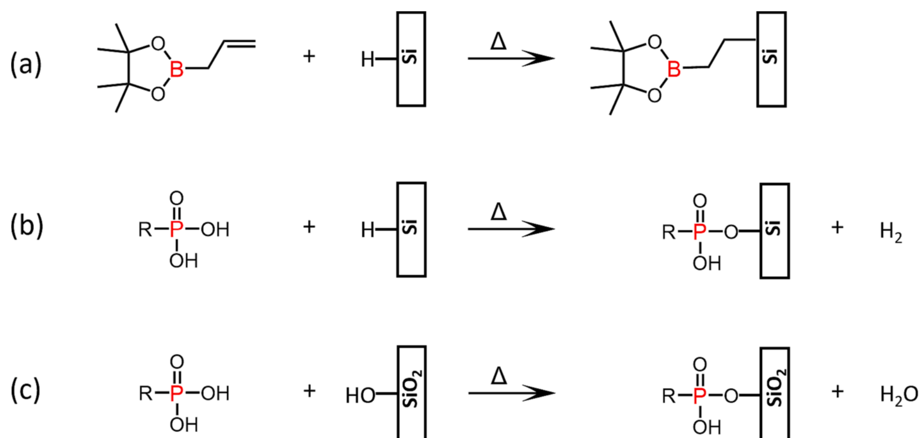

Fig. 2. Some reaction classically used in MLD processes.

pinacol ester. Another class of molecules that are particulary used for P doping processes are phosphonic acids [28,30], for which the reaction with the silicon surface was initially not well understood. A peculiar mechanism, which results in the production of H_2 molecules as by-products, was proposed by Longo et al. [36] on the basis of several studies previously conducted on the reaction between alcohols and hydrogen-terminated silicon surfaces [35,37,38,39,40]. Such reaction is represented in Fig. 2 **(b)** in the case the reactive molecule is a generic phosphonic acid. Furthermore, the authors demonstrated that P-C bonds are less thermally stable than P-O bonds. Therefore, while the organic part of the dopant molecules is fully degraded at temperatures higher than 500 °C, the resulting P-containing species are stabilized by inclusion within the silicon lattice. In this perspective, the SiO_2 capping layer results unnecessary.

Finally, since oxide-free silicon surfaces requires dangerous treatments with hydrofluoric acid (HF), MLD processes on native silicon oxide were introduced. The main way to produce self-assembled monolayers of P-containing molecules on SiO_2 is the condensation reaction occurring between phosphonic acids and silanols (see Fig. 2 **(c)**). In particular, dry adsorbed films of such molecules are generally obtained through the so-called *tethering by aggregation and growth (T-BAG)* method and the condensation is then promoted by thermal annealing at ~ 150 °C [41,42,43]. In 2018, Longo et al. reported that such monolayer can be used to introduce dopant phosphorus in silicon without preliminary removal of the native oxide [44]. In particular, TOF-SIMS analyses demonstrated that the diffused P atoms are about the same amount present in the monolayer. Furthermore, temperatures above 700 °C completely degrade the organic part of the molecules by driving the diffusion of P atoms into silicon. As in the case previously described, the SiO_2 capping layer results unnecessary.

Although promising results towards precision doping were obtained through the MLD technique, some drawbacks are nevertheless present. First of all, the reactions between dopant molecules and surfaces are generally conducted in solution, thus providing for the management of considerable quantities of organic solvents with the consequent problems of disposal and purification. Furthermore, reaction kinetics are typically slow and long times are required to guarantee the formation of a complete monolayer. Second, carbon impurities are generally introduced in silicon due to the organic parts of the dopant molecules [45,46]. Such defects were demonstrated to be responsible for the electrical deactivation of more than 20 % of the included P atoms [47]. Finally, since the footprint of the used dopant molecules is difficult to vary drastically so that recurring areal density of ~ 10^{14} molecules/cm^2 (1 molecule/nm^2) are generally obtained, a wide modulation of the

dopant dose is prevented, unless using complex molecular architectures [48].

The emerging technology of *polymeric precision doping (PPD)*, which is presented in this review, has been developed with the aim of overcoming the difficulties of the classical MLD method. Small dopant molecules of MLD are replaced with polymeric carriers with tunable molecular weights which are chemically bonded onto silicon through the well-known *grafting to* process. The theory underlying *grafting to* reactions will be discussed in chapter 2. The workflow of the PPD process and the first generation of dopant polymers described in literature will be presented in chapters 3 and 4, respectively. The effect of molecular weight dispersity in PPD processes will be discussed in chapter 5, whereas the opportunities offered by precision polymers, such as polypeptides and polypeptoids, will be explained in chapter 6. Finally, future perspectives will be contained in chapter 7.

2. *Grafting to* reaction: A general introduction

The *grafting to* reaction consists in the chemical anchoring of an end-functional polymer onto a substrate [49], such as silicon or silicon oxide, as schematized in Fig. 3 **(a)**. Thin films of polymers chemically bonded to the surface by one chain-terminal are generally referred as *polymer brushes*. The capability to drastically modify the underlying surface currently gives polymer brushes a privilege role in various research fields, from biomedical sciences [50] to electronics [51,52]. For example, polymer brushes consisting of poly(styrene-st-methyl methacrylate) P(S-st-MMA) statistical copolymers were used to neutralize SiO_2 surfaces in order to vertically align molecular patterns obtained by self-assembling block-copolymers in nanolithography applications [53,54,55,56,57].

The main advantage of the *grafting to* reaction is its *self-limiting nature* [49], meaning that the number of polymer chains contained in a brush cannot exceed a maximum value which is reached when the brush thickness (H) approaches or overcomes two times the radius of gyration (R_g) of the employed polymer [58]. In Fig. 3 **(b)** the grafting kinetics of a hydroxy-terminated P(S-st-MMA) and a diethyl phosphate-terminated polystyrene (PS) on SiO_2 substrates are reported as a typical example [59]. Both systems are characterized by a fast increase of the brush thickness during the shortest reaction time, until the rate of the growth slows down and finally stops for sufficiently long times, where H approaches the typical value of $2R_g$. Consequently, polymer chains in brushes obtained by *grafting to* reactions are in random coil or weakly stretched configurations.

The physical mechanism underlying the self-limiting nature of *grafting to* reactions is widely debated in literature and not fully understood yet. Several authors, such as Luzinov [60] and Iyer [61], argued that the grafting reaction proceeds if the thickness of the formed brush is low enough to allow additional polymers to reach the surface without requiring excessive stretching of the polymer chains. For $H \sim 2R_g$ the chain stretching becomes relevant and the diffusion of new reactants to the surface is prevented. On the contrary, an alternative vision assumes that the brush thickness approaches a plateau value when the reaction reaches a thermodynamic equilibrium [62,63,64,65,66,67]. At this point, grafting and degrafting reactions proceed with the same rate and thus the brush does not grow anymore. In the recently published review on *grafting to* reaction mechanism [68], Chiarcos et al. examined a relevant number of experimental systems in which thermodynamic equilibrium seems to be the best hypothesis to explain the nature of such processes.

Besides being a question of purely theoretical nature, the self-limiting behavior of *grafting to* reactions also has fundamental implications from a technological point of view. This is due to the quantitative relation between H and the *grafting density (Σ)* of the brush, which is the number of grafted chains for unit of area. Such relation is reported in **Equation (1)**,

$$\Sigma = \frac{HdN_A}{M_n} \tag{1}$$

where d is the polymer density, N_A is the Avogadro's number and M_n is the number average molecular weight of the grafted polymer. Since d and M_n are defined parameters and, for long enough times, H was observed experimentally to converge to the plateau value of $2R_g$, the grafting density of the brush is expected to scale according to the

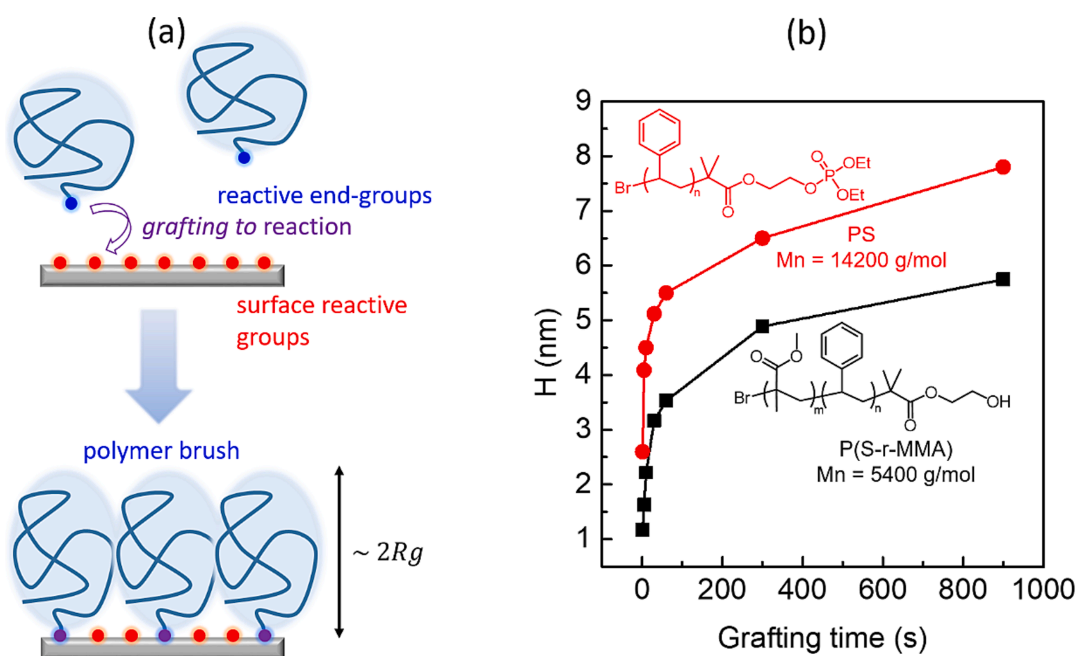

Fig. 3. (a) Grafting to reaction representation. (b) Brush thicknesses (H) as a function of the grafting time for a hydroxy-terminated P(S-st-MMA) with M_n = 5400 g/mol [58] and a diethyl phosphate-terminated PS with M_n = 14200 g/mol [59]. In the first case the grafting reaction occurs through the condensation between the hydroxyl group and silanols present over a SiO_2 surface, whereas in the second case the reaction is a *trans*-esterification of the diethyl phosphate group also with silanols on SiO_2. Both reactions were conducted at 250 °C.

following equation

$$\Sigma \sim \frac{1}{M_n^{0.5}} \tag{2}$$

which is obtained considering that, for a random coil, R_g is proportional to $M_n^{0.5}$. It is important to underline that the above relationship between Σ and M_n refers only to brushes obtained by *grafting to* reactions. **Equation** (2) suggests that Σ can be properly tuned by simply changing the molecular weight of the polymer, consistently with data available in the literature [68].

In the perspective of precision doping of silicon, polymers with a reactive terminal-group containing a dopant atom, as in the case of the phosphate-terminated polystyrene, can be grafted on silicon/silicon oxide as an alternative to the small molecules used in MLD approaches. In this way, the number of grafted molecules (Σ) and, consequently, the number of dopant atoms, can be tuned simply by changing the molecular weight of the polymeric part of the molecule. Areal P dose differences of more than one order of magnitude can then be reached with the PPD approach, overcoming one of the more pressing problems previously highlighted for the MLD. The entire workflow of the PPD technology, which develops around the fundamental *grafting to* reaction, will be described in the next chapter.

3. Polymeric precision Doping: Workflow of the process

The workflow of PPD is essentially developed in six steps which are schematically depicted in Fig. 4. Clean wafers exposing silanols (step 1) are coated by thin films of dopant polymer with thicknesses that are sufficiently high (>20 nm) to avoid thermal induced dewetting phenomena [57] (step 2). The *grafting to* reaction is then promoted by thermal annealing until polymer brushes with H ~ $2R_g$ are obtained (step 3). Although it was demonstrated that residual traces of solvent remain trapped in the polymer film [69,70,71], the subsequent grafting reaction can be considered as effectively carried out in dry conditions. This fact has essentially three considerable technological advantages. Firstly, since in polymer melt excluded volume interactions are screened out allowing the chains to interpenetrate, higher grafting densities are generally obtained with respect to *grafting to* reaction conducted in solution, in which polymer coils are mutually exclusive [72]. Secondly, grafting reactions are considerably faster than the classical reactions reported for MLD technologies due to higher reactant concentrations. The thermal annealing step is generally conducted by Rapid Thermal Annealing (RTA) processes and it was demonstrated that polymer brushes at the plateau thicknesses are obtained in less than 900 s, which is a time considerably lower compared to the many hours of MLD [58,73]. Finally, the use of organic solvents is confined to the spin-coating process and then remarkably reduced compared to MLD procedures. Subsequently, unreacted chains are removed by several sample washes (step 4), typically carried out in toluene, and the organic part of the grafted molecules is then removed by oxygen plasma treatment (step 5). Etch rates of 0.03 and 0.06 nm/s were reported for PS and PMMA, respectively [59]. The complete removal of the organic part of the brush avoids carbon contaminations which are often observed in MLD processes.

Finally, a protective SiO_2 layer is deposited on the samples by electron-beam evaporation (step 6), resulting in a confined dopant atom δ-layer, on which dopant atom quantification can be performed by TOF-SIMS analyses [45]. Dopant atom diffusion in silicon is then promoted by RTA processes at temperatures higher than 1000 °C, as in the standard MLD procedures.

In conclusion, the PPD process is presented as an improvement of the classical MLD method, with the further benefit of being based on procedures and technologies already implemented in microelectronic industry.

4. Polymeric precision Doping: A review of the first generation of dopant polymers

The PPD procedure was for the first time described in a seminal paper by Perego et al. in 2018[59]. Diethyl phosphate-terminated PS and PMMA polymers, conveniently defined as PSn-P and PMMAn-P, with molecular weights ranging from 2.3 to 25.4 kg/mol, were used as dopant molecules (see Fig. 5 **(a)** for the complete chemical structures). Such samples were obtained starting from the corresponding hydroxy-terminated polymers, synthesized by *Atom Transfer Radical Polymerization (ATRP)*, subsequently reacted with diethyl chlorophosphate to perform the phosphorylation of the hydroxyl-terminal group.

The *grafting to* reaction of PSn-P and PMMAn-P polymers was carried out on silicon wafers covered by ~ 10 nm thick layers of SiO_2, similar to the reaction reported in Fig. 2 **(c)**. The process was performed at 250 °C by RTA process and H ~ $2R_g$ were obtained for all polymers in 900 s. In Fig. 5 **(a)** the plateau H values are reported as a function of M_n. The data are in remarkable agreement with the H ~ $M_n^{0.5}$ law, which is expected considering R_g ~ $M_n^{0.5}$ in random coils. Furthermore, H can be introduced in **Equation** (1) to calculate the grafting density (Σ) of each sample.

The removal of the organic part of the brushes was performed by plasma etching and a ~ 10 nm thick capping layer of SiO_2 was deposited

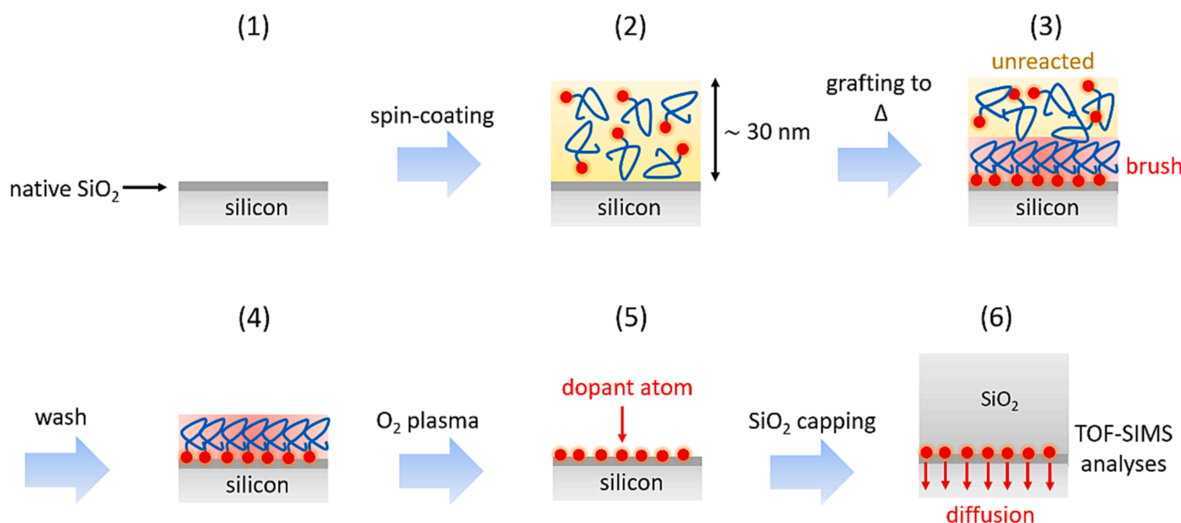

Fig. 4. Workflow of the polymeric precision doping (PPD) process.

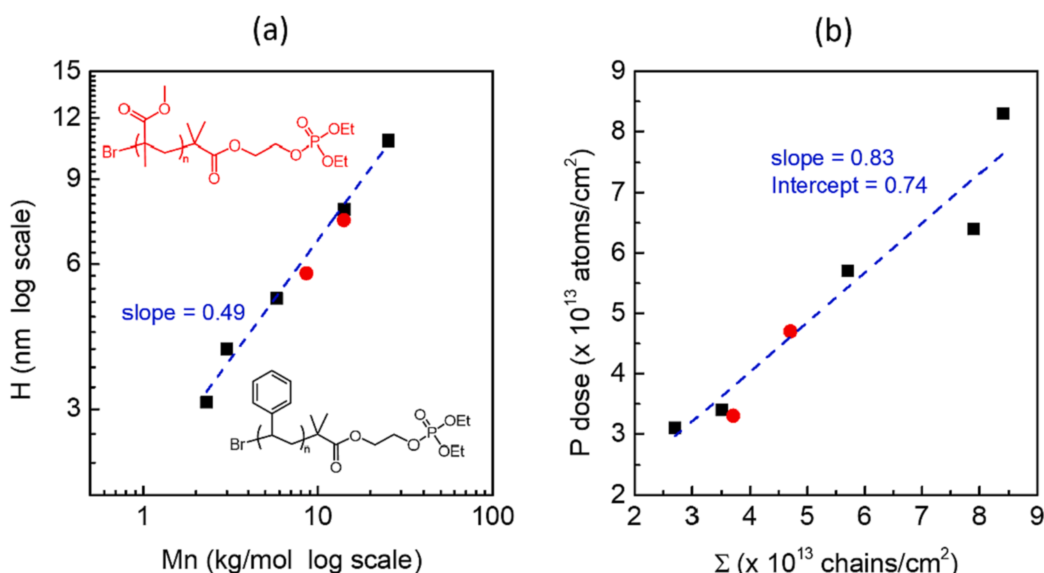

Fig. 5. (a) Plateau thickness (H) as a function of the M_n of the grafted PSn-P (black squares) and PMMAn-P (red circles) polymers. Chemical structures are also included. **(b)** P dose, measured by TOF-SIMS analyses, as a function of the calculated Σ. Linear fit of the data are included (dashed blue lines).

over the samples. Phosphorus atoms then result trapped in a δ-layer included in a ~ 20 nm thick matrix of SiO_2. P dose quantification was performed by TOF-SIMS analyses. In Fig. 5 **(b)** the measured P dose is reported as a function of the calculated Σ for each sample. A one-to-one correspondence between the P dose and Σ is observed, confirming that each chain in the brush contributes to carry a single P atom onto the substrate. Furthermore, Fig. 5 **(b)** clearly demonstrates that the P dose can be finely tuned by changing the molecular weight of the dopant polymer, making accessible areal dopant concentrations ranging from 2 to 9×10^{13} atoms/cm^2 (from 0.2 to 0.9 atoms/nm^2) thus expanding the range of accessible P dosages in comparison to the classical MLD technology. Unfortunately, it is difficult to obtain areal dopant concentrations higher than 10^{14} atoms/cm^2 due to the extremely low molecular weight required for the dopant polymers. However, it is possible to overcome this drawback by repeating the grafting/etching cycles. A stepwise regular increase in the P amount is observed after each cycle. In this perspective, the upper limit of the P dose is provided by the number of available silanols present on the surface.

P diffusion in silicon was carried out by RTA processes at temperatures ranging from 1000 to 1250 °C for 5 s and P profiles were then monitored by TOF-SIMS analyses. Significant P drive-in was observed only for temperatures higher than 1100 °C due to the low-diffusion barrier formed by the SiO_2 layer. The total amount of injected phosphorus was estimated by TOF-SIMS profile integration and only 50 % of the P atoms present in the δ-layer result effectively diffused in silicon, while the remaining 50 % are trapped in SiO_2. Such number is considerably increased when the *grafting to* reaction is performed on ~ 2 nm thick native SiO_2 layer, thus reducing the oxide diffusion barrier. In this case, Perego at al. [74] reported activation efficiencies (η) of ~ 80 % by Hall measurements. This fact is theoretically explained by the Altermatt model, which asses that, for P concentrations higher than 10^{17} atoms/cm^3, only a fraction of the substitutional P atoms are effectively ionized, even at room temperature [75]. Surprisingly, complete ionization (η = 100 %) was observed by the same author in samples prepared by grafting PSn-P and PMMAn-P polymers directly on deglazed silicon, with a reaction similar to that reported in Fig. 2 **(b)** [76,77]In these cases, the Altermatt model seems to be no longer valid, whereas more accurate predictions are provided by the alternative model proposed by Li et al. [78], in which η ~ 95 % is calculated. Such differences in dopant activation for samples prepared by using either deglazed silicon or on silicon oxide indicate an at least incomplete understanding of the drive-in process of P atoms. In any case, the η values obtained by PPD process are higher than the MLD ones, which are assessed around 70 %[30], and comparable with the ones currently obtained through ion implantation technology, confirming the actual potential of this new method in silicon doping processes. These data indicate that the this first generation of P-terminated polymers represents a valuable tool to properly modulate conductivity of the silicon substrate by a gentle doping approach.

Later on, a one-pot synthetic strategy for the preparation of dopant polymers was proposed by Chiarcos et al. [79]. In this approach, N-*tert*-butyl-N-[1-diethylphosphono(2,2-dimethylpropyl)] nitroxide (SG1) was employed both as P source and free radical controller in the *Nitroxide Mediated Polymerization (NMP)* of styrene as illustrated in Fig. 6 **(a)**). These polymers were marked as PSn-SG1. Remarkably, this synthetic procedure does not include metal catalysts which can severely limit the use of dopant polymers in microelectronic industry due to their highly contaminating nature and which are indeed present in ATRP [80].

Grafting to reactions were conducted using PSn-SG1 samples with M_n ranging from 2.5 to 52 kg/mol at 250 °C in a RTA apparatus. For each polymer, the plateau value of H is reached in ~ 200 s and, surprisingly, thicknesses significantly lower than the expected $2R_g$ value were obtained. In Fig. 6 **(a)**, H values obtained at 900 s for PSn-P and PSn-SG1 samples are compared. On one hand, values of H systematically lower were obtained when PSn-SG1 polymers were used. For example, if a brush ~ 7.8 nm thick was obtained for the PSn-P sample with M_n = 14.2 kg/mol, only 2.85 nm of polymer was observed when the PSn-SG1 sample with M_n = 12.3 kg/mol was used. Furthermore, in the PSn-SG1 case, H plateau values converge to ~ 3.2 nm for M_n higher than 12.3 kg/mol and do not follow the expected $H \sim M_n^{0.5}$ law, which well represents the data of PSn-P polymers. These data clearly indicate that PSn-SG1 polymers follow a grafting mechanism that is fundamentally different from what is normally reported in literature.

On the other hand, the P doses, measured by TOF-SIMS analyses after plasma etching and SiO_2 capping, perfectly fit the grafting densities estimated with **Equation** (1), as it is represented in Fig. 6 **(b)**. This means that, despite a different grafting mechanism, PSn-SG1 and PSn-P polymers act as dopant molecules in an identical fashion, carrying on the substrate a single P atom for each grafted chain. Furthermore, this new system makes accessible Σ values lower than 3×10^{13} chains/nm^2 which are generally forbidden for PSn-P systems due to the critical issues associated with the use of very large polymers, widening the range of PPD possibilities.

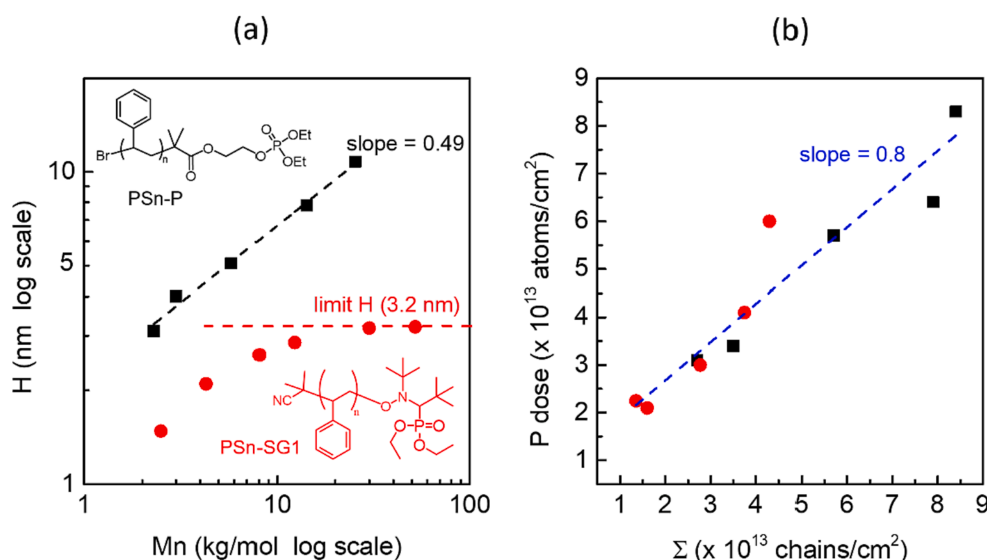

Fig. 6. (a) Plateau thickness (H) as a function of the M_n of the grafted PSn-P (black squares) and PSn-SG1 (red circles) polymer. Chemical structures are also included. **(b)** P dose, measured by TOF-SIMS analyses, as a function of the calculated Σ. Linear fit of the data are included (dashed blue lines).

An in-depth investigation of the grafting mechanism of PSn-SG1 polymers was carried out by using *Direct Exposure Probe (DEP)* analyses [81]. In this technique, thin polymer films are deposited on a peculiar filament which allows the samples to be heated with thermal treatment similar to the RTA one. Degradation products are then collected and directly analyzed by mass spectrometry, thus providing a time-map of the polymer degradation. Interestingly, at 250 °C the molecular fragment related to the degradation of the SG1 moiety completely evolves from the polymer film in 200 s, which is exactly the time observed for the formation of brushes at the plateau thicknesses. This data suggests that two competing events occur during the *grafting to* process: the thermal degradation of the reactive terminal-group of the PSn-SG1 polymers, probably triggered by the thermolable C-O-N bond that links the SG1 group to the main chain, and the effective grafting of the undegraded chains. A schematic picture of the process is provided in Fig. 7. It was estimated that about 10 % of the polymers contained in the initial layer is grafted onto the substrate, whereas the other 90 % degrades after 200 s of thermal treatment.

Finally, an increase of the grafting temperature was demonstrated to further decrease the percentage of undegraded-grafted chains, thus reducing the amount of P atoms carried on the substrate. Temperature and polymer molecular weight are thus experimental variables that can both be modulated in order to finely control the dopant dose.

In conclusion of this chapter, the effectiveness of PPD technology can be argued, in particular by observing that all the criticism underlying the classical MLD approach, from the slow reaction kinetics to the narrow range of accessible dopant doses, are effectively overcome. However, a finer control issue seems to be intrinsically realted with this innovative doping system, which could be defined as the molecular weight dispersity effect. Such problem will be discussed in detail in the next chapter.

5. Molecular weight dispersity effect

Molecular weight dispersity indicates the coexistence of a broad range of oligomers with different molecular weights within the same sample and it is an ubiquitous phenomenon in all synthetic polymers. When **Equation** (1) is used to estimate the grafting density of a polymer brush, the M_n of the polymer in the brush is assumed to be equal to the M_n of the initial polymer. In other words, it is generally assumed that the polymer molecular wight distributions are conserved during *grafting to* processes. Although this may be considered as a good approximation for polymers with small molecular weight dispersity, such as samples obtained by controlled radical polymerizations, slight but unequivocal shifts have been recently reported in literature. For example, Michalek et al. recently demonstrated the preferential inclusion of shortest chains in polymer brushes obtained by *grafting to* reactions conducted in solution between functionalized PMMA and silica particles [82,83].

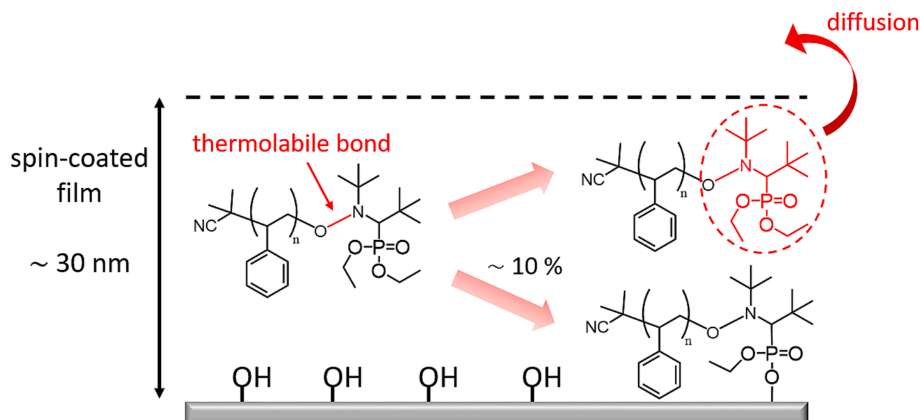

Fig. 7. Representation of the grafting and degradation mechanisms observed for PSn-SG1 samples.

Molecular weight distributions and M_n values shifted toward lower weights were then registered for the grafted polymers with respect to the initial samples.

Detailed studies on the molecular weight dispersity effect in *grafting to* reactions conducted in dry conditions was recently published by Chiarcos et al. [84,85,86]. To exacerbate the effect, equimolar blends containing two hydroxy-terminated P(S-st-MMA) polymers with different molecular weights were used. In particular, half of the molecules consists in a partially deuterated polymer with $M_{n,\ Rd11.2} = 11.2$ kg/mol and the other half of fully hydrogenated polymers with $M_{n,\ Rn}$ ranging from 3.6 to 38.6 kg/mol. Chemical structures and molecular weights are reported in Fig. 8 **(a)**.

The blends were grafted on SiO_2 substrates for times ranging from 10 to 1800 s and at temperatures ranging from 190 to 250 °C. Unreacted chains were removed by toluene washes and the obtained brushes were characterized by ellipsometry and a *thermogravimetric analysis-gas chromatography-mass spectrometry (TGA-GC–MS)* apparatus. Such hyphenated system allows to quantify the mass fractions of deuterated and hydrogenated species in the brush, thus making possible to calculate the partial grafting denisties of deuterated ($\Sigma_{Rd11.2}$) and hydrogenated (Σ_{Rn}) polymers. In Fig. 8 **(b)** the brush fraction of hydrogenated chains, indicated as Σ_{Rn} / (Σ_{Rn} + $\Sigma_{Rd11.2}$), are reported as a function of the grafting time for the experiments carried out at 250 °C. Considering that the fraction of hydrogenated chains is 0.5 in the initial equimolar blend, a systematic enrichment of the component with lower molecular weight is observed. In fact, for $M_{n,\ Rn} < M_{n,\ Rd11.2}$, brush fraction of hydrogenated chains equal to 0.64, 0.60 and 0.52 were registered when the hydrogenated polymers had $M_{n,\ Rn}$ equal to 3.6, 5.4 and 8.7 kg/mol, respectively. On the contrary, in the $M_{n,\ Rn} > M_{n,\ Rd11.2}$ cases, the brush fractions were 0.40 and 0.34 when $M_{n,\ Rn}$ were 19.9 and 38.6, respectively. Interestingly, the degree of enrichment seems to depend only from the molecular weights of the two components of the blend and does not change with the grafting time. Furthermore, the authors demonstrated that also the grafting temperature does not play a significant role in the phenomenon.

Remarkably, the short chain enrichment can be quantitatively related with the molecular weights of the polymers by the empirical **Equation (3)**, as showed in Fig. 8 **(c)**.

$$\frac{\Sigma_{Rn}}{\Sigma_{Rd11.2}} = \left(\frac{M_{n,Rn}}{M_{n,Rd11.2}}\right)^{-0.55} \tag{3}$$

Equation (3) was recently justified considering the relation occurring in *grafting to* reactions between the kinetic constant (k) and the molecular weight of the polymer [68], which was proposed by Kim et al. [65]. The reported relation $k \sim M_n^{-0.55}$ considers the entropy penalty needed to confine a terminal group close to the surface, as required in grafting reactions, and directly provides the explanation of the lower grafting kinetics observed for polymers with higher molecular weights. A generalized version of **Equation (3)** was also provided by Chiarcos et al. for *grafting to* reactions of binary polymer blends with arbitrary initial composition [68]. The preferential grafting of short chains was confirmed in all cases.

Unfortunately, the study of the molecular weight dispersity problem for dopant polymers is at a more backward level than that of hydroxy-terminated systems. Furthermore, the available data seem to indicate a more complex scenario. Some speculation concerning the effect of molecular weight dispersity in the *grafting to* reaction of dopant polymers is contained in the recent work of Perego et al. [87]. Here, diethyl phosphate-terminated poly(methyl methacrylate) polymers, of the same type of the PMMAn-P samples reported in Fig. 5 **(a)**, were grafted onto SiO_2 at 250 °C, unreacted chains are removed and P dose was measured by TOF-SIMS analyses after plasma etching and SiO_2 capping, as described in chapter 4. The grafting density, calculated by **Equation (1)**,

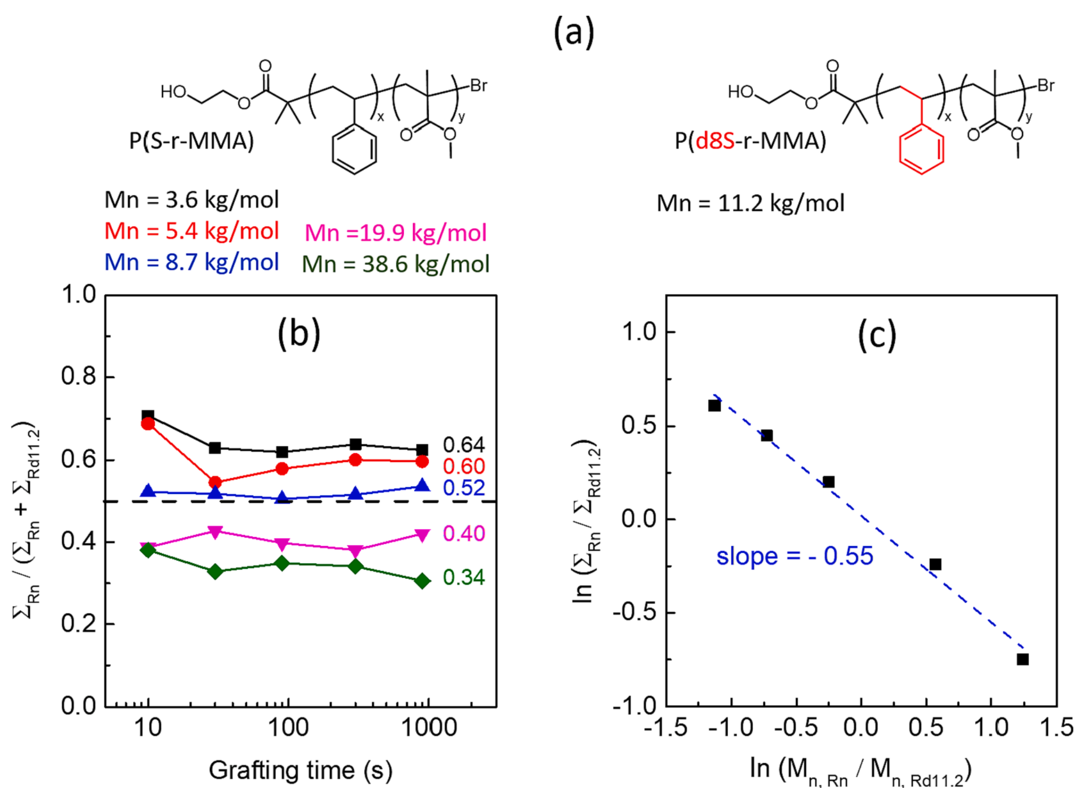

Fig. 8. (a) Chemical structures and molecular weights of the hydroxy-terminated polymers making up the blends. **(b)** Molar fraction of fully hydrogenated polymers in the grafted brushes as a function of the grafting time. The experiments were carried out at 250 °C. The fraction average values are also included. **(c)** Molar ratio between the number of hydrogenated and deuterated chains in the brushes as a function of the ratio between their molecular weights. The best fit line is also included.

and the measured P dose for a PMMAn-P sample with $M_n = 7.5$ kg/mol are reported in Fig. 9 **(a)** as a function of the grafting time. Firstly, the Σ value and the P amount at 900 s are different, in contrast to what is generally observed for similar systems (see Fig. 5 **(b)**). In particular, a P dose of 3.8×10^{13} atoms/cm^2 (0.38 atoms/nm^2) corresponds to a much higher Σ of 5.51×10^{13} chains/cm^2. Moreover, a decreasing trend of the P dose was observed with increasing time of grafting, in the opposite direction of the temporal increase of H and, consequently, of Σ. A similar discrepancy between Σ and the P dose was also observed in samples prepared at different temperatures, ranging from 190 to 270 °C, for 900 s, as reported in Fig. 9 **(b)**. From one hand, H and Σ increases with temperature, as expected. On the contrary, the P dose follows an inverse trend, with values decreasing from 4.4 to 2.6×10^{13} atoms/cm^2 for the samples obtained at 190 and 270 °C, respectively.

Since thermal degradation phenomena were excluded by MALDI-TOF analyses, which were performed on the unreacted chains removed after the grafting process, the differences between Σ and P were attributed to the fact that each polymer contains oligomers with different molecular weights, in other words to an effect of molecular weight dispersity. The authors suggest that during the first times of reaction the shortest chains constituting the sample react preferentially, thus producing thin layer (small H) containing a large number of small grafted chains and, consequently, a large number of dopant atoms. As the reaction proceeds, a dynamic exchange would lead to the grafting of longer chains, with consequent increase of H and decrease of P. In this perspective, the same polymer sample produces grafted brushes with M_n that is function of time, low for short times and then higher, making the use of **Equation (1)** infeasible. Since the Σ values reported in Fig. 9 are obtained by using such equation and considering the M_n of the polymer in the brush equal to the one of the initial sample, they result systematically under/overestimated. A similar mechanism could come in to play in the experiments carried out by changing the grafting temperature.

Since no deeper explanations are reported in literature, we speculate about a tentative model explaining how this time/temperature dependence of the grafted chain dimension could occur. Firstly, it is necessary to consider the reaction environment. Polymers terminated with highly polar phosphate groups are deposited on a polar surface, that is SiO_2 exposing surface silanols. It is possible to assume that, during the spin-coating process, a preferential absorption of short chains occurs at the SiO_2/polymer interface. Such adsorption could provide a reduction of the surface tension and, in this perspective, short chains are preferred due to the higher packing which thus produces better surface screening. As the system is heated to promote the grafting reaction, the high concentration of short chains at the surface will produce a brush containing predominantly polymer with low molecular weights. Since *grafting to* reactions are conducted at high temperatures, the energetic gain of the adsorption results quickly less relevant, where the weight distribution at the interface becomes more homogenous due to entropic reasons. As the reaction environment at the interface is changed, also the brush composition will be dynamically driven to a more homogenous composition, including both short and long chains and resulting in higher H and lower effective Σ. This loss of adsorption results faster and cleaner at higher temperatures, thus producing the results reported in Fig. 9 **(b)**. A schematic representation of this highly speculative scenario is shown in Fig. 10.

This vision also seems to be compatible with some results recently published on the grafting of a PSn-P polymer, with $M_n = 2.3$ kg/mol, on both deglazed and not-deglazed (i.e. covered by native SiO_2) silicon [76]. On the one hand, thicker brushes were obtained for grafting process performed on deglazed silicon. In fact, H values of 3.2 and 2.4 nm were obtained respectively on deglazed and not-deglazed silicon after 900 s. On the other hand, a higher amount of P was observed onto the not-deglazed sample, resulting in a P dose of 6.01×10^{13} atoms/cm^2, which is more than two times the 2.81×10^{13} atoms/cm^2 value measured for the deglazed sample. In the perspective discussed before, the SiO_2 polar layer which cover not-deglazed silicon should promote the adsorption of the shortest chains contained in the PSn-P sample, thus providing thin brushes and high P doses. On the contrary, the apolar surface of deglazed silicon should promote a depletion of polar groups and short chains at the interface, thus favouring the grafting reaction of the longest chains. Further data are undoubtedly necessary to fully define the role of molecular weight dispersity in PPD processes. For example, blends of short and long dopant polymers could be used as done in the case of hydroxy-terminated P(S-st-MMA) described above. Furthermore, recently published synthesis techniques [88–93] pave the way for the production of polymers with molecular weight distributions that are controlled in both width and skewness thus providing a whole new set of tools that can be implemented in the study of such complex systems.

Regardless of the validity of the suggested model, it is clear that *grafting to* reactions are intrinsically not trivial in the case of disperse polymers, in particular in presence of highly polar terminal groups such as in dopant polymers. Fine control of dopant dose then requires an accurate control of the grafting parameters, such as temperature and time, and no general equation, such as **Equation (1)**, can be used with

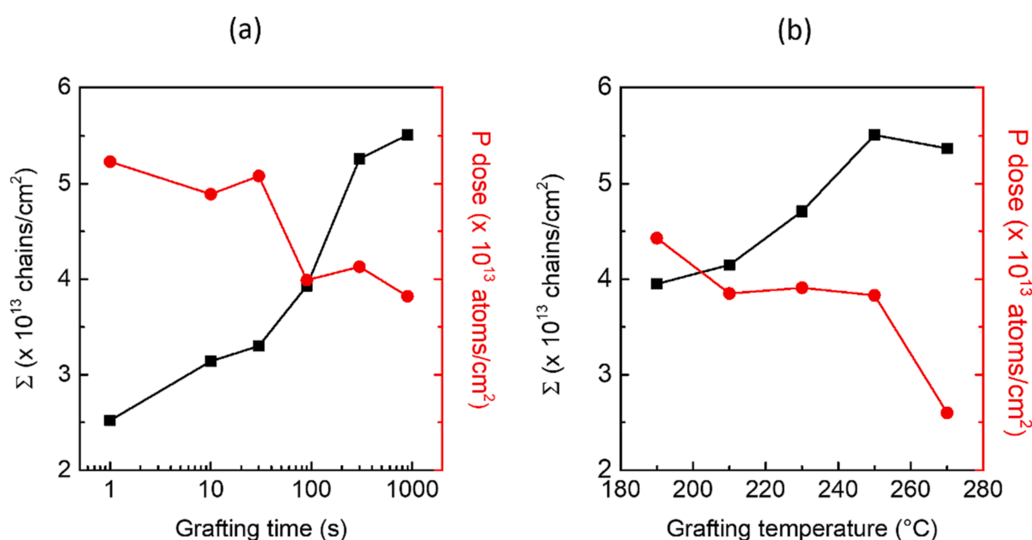

Fig. 9. **(a)** Grafting density and P dose of the grafted PMMAn-P sample with $M_n = 7.5$ kg/mol as a function of the grafting time. The experiments were carried out at 250 °C. **(b)** Grafting density and P dose of the same polymer after 900 s as a function of the grafting temperature.

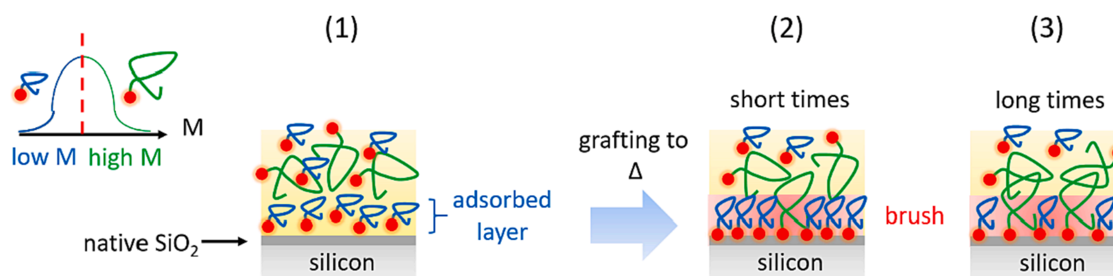

Fig. 10. Speculate mechanism underlying the *grafting to* reaction of PMMAn-P polymers: (1) surface adsorption of short chains, (2) grafting of short chains occurring at short times and (3) dynamical exchange between short and long chains until equilibrium is reached.

complete confidence. An overall solution to all these problems has recently been identified in the use of truly monodisperse dopant polymers, which will be discussed in detail in the next chapter.

6. Bioinspired polymers: The final stage of PPD

Unlike their synthetic counterparts, some natural polymers, such as polypeptides and polynucleotides, are characterized by perfect control over the number and the structure of monomeric units making up the molecule. In 1984 Robert Merrifield was awarded the Nobel Prize in Chemistry for a synthetic protocol that emulates the natural process of perfectly controlled synthesis of polypeptides [94]. This method is generally called *Solid-Phase Synthesis (SPS)* and consists in growing polymers starting from solid particles of functionalized resin by adding one monomer at a time. In 1992, SPS approach was extended by Zuckermann et al. to the synthesis of polypeptoids [95], which are macromolecules similar to polypeptides but with side groups bonded to nitrogen instead of α-carbon. The chemical structure of a generic polypetoid is reported in Fig. 11 **(a)**. The lack of hydrogen bond donors makes such molecules generally soluble in standard organic solvents, thus increasing their processability. A schematic representation of SPS method applied to polypeptoid synthesis is reported in Fig. 11 **(b)** [96]. Resin particles exposing amine groups (1) are reacted with bromoacetic acid solution containing *N, N'*-Diisopropylcarbodiimide (DIC) as a catalyst to produce the corresponding amide (2). Unreacted molecules are removed and the resin is washed several times by fresh solvent. The resin is then immersed in an amine solution where the substitution of the amine for the bromine group take places (3). The solid phase is again washed with fresh solvent. This cycle is then iterated many times to obtain the final polypeptoid. Remarkably, both the number of units and the nature of the side groups (R) can be controlled by selecting the number of cycles and the nature of the amines, respectively.

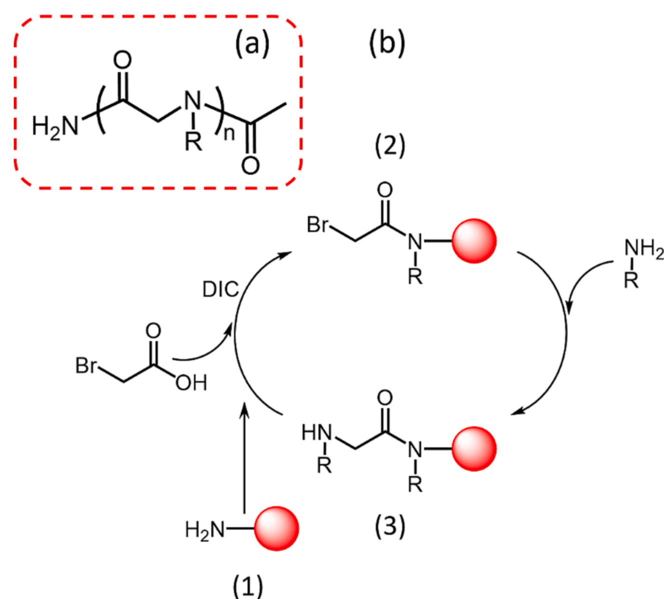

Fig. 11. (a) Chemical structure of a generic polypeptoid. **(b)** Schematic representation of SPS approach applied to polypetoid synthesis.

The revolutionary opportunity to synthesize molecules with discrete molecular weights and including a large plethora of functional groups was recently exploited for PPD applications by Ospina et al. [97]. Polypeptoids with 5, 10, 14 and 19 repeating units, of which the terminal one contains a dopant phosphonate group, and thus with molecular weights (M) ranging from 0.84 to 3.11 kg/mol were synthesized by SPS protocol implemented on an automatic polypeptide synthesizer. Molecular structures and MALDI-TOF spectra are reported in Fig. 12 **(a)** and **(b)**, respectively.

All samples were then spin-coated on silicon substrates covered by ~ 10 nm thick SiO_2 layers and *grafting to* reactions at different temperatures were performed. A broad range of temperatures from 120 to 250 °C was evaluated and in each case degradation phenomena were observed after a specific time. This fact was attributed to the low thermal stability of polypeptoids for which TGA measurements showed weight losses at approximately 200 °C. Fortunately, high temperature experiments confirmed that polymer brushes at the plateau thickness can be obtained before polymer degradation occurs. In particular, 190 °C and 40 s were identified as the ideal condition to obtain intact brushes at the plateau thickness. In Fig. 12 **(c)** H values obtained in such conditions are reported as a function of the molecular weight of the polypeptoid. H and M values can be related by the law $H \sim M^{0.72}$, in which the exponent is slightly higher compared to the classical 0.5 value. This fact could be related to chain rigidity which becomes not neglectable in polymers with low molecular weights such as those considered here. Finally, P doses were evaluated by TOF-SIMS analyses after the routine solvent washes and plasma etching. The data are reported in Fig. 12 **(d)** as a function of M and indicate a marked decrease of P as M increases. More precisely, P dose is 9.8×10^{13} atoms/cm^2 (0.98 atoms/nm^2) for the 5 unit polypeptoid and decreases to 4.3 9.8×10^{13} atoms/cm^2 when the unit number increases to 19. It therefore appears clear that polypeptoids can be successfully implemented in PPD processes, with the advantages of being perfectly determined and synthesized in an automatic and totally reproducible way.

7. Future perspectives of PPD

From the digression in the PPD field carried out in this short review, it is evident that extremely promisingly results have already been obtained, highlighting the possibility to implement the proposed methodology at laboratory scale as a reliable and low-cost alternative to conventional doping approaches. The proposed approach offers the possibility to develop simple protocols for the fabrication of junctions or more complex semiconductor devices even in research structures where no ion implanters are available. Nevertheless, some unsolved issues still remain and need to be addressed before PPD can be consider solid enough to be implemented at industrial level.

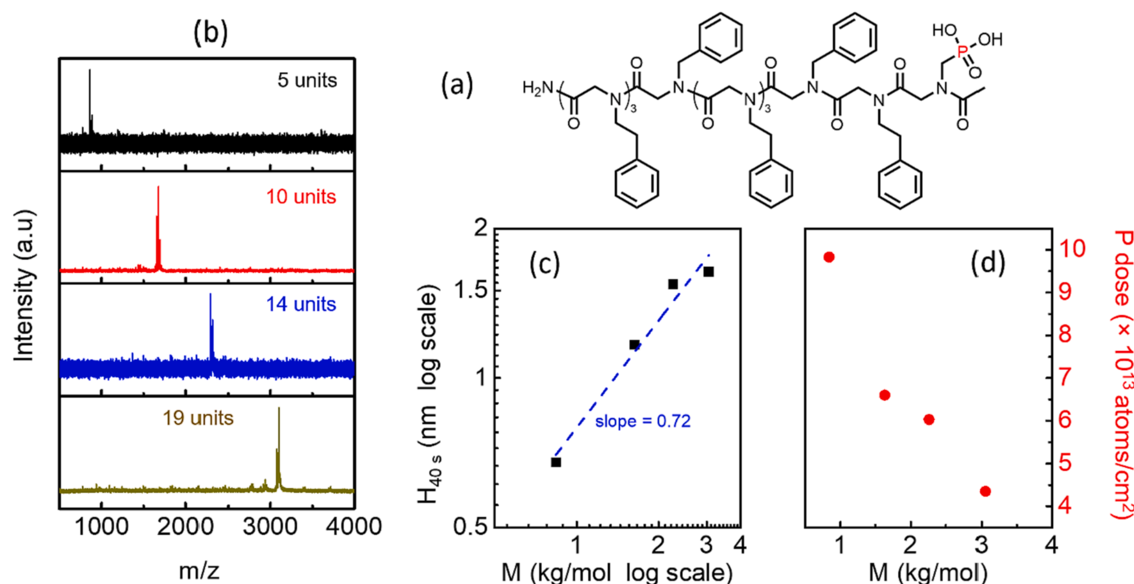

Fig. 12. **(a)** Chemical structure of the dopant polypeptoid consisting of 10 units. **(b)** MALDI-TOF spectra of dopant polypeptoids with 5, 10, 14 and 19 units. **(c)** H values collected at 190 °C after 40 s as a function of M. Best linear fit is also included. **(d)** P dose measured by TOF-SIMS analyses as a function of M.

First of all, the physico-chemical mechanisms underneath the *grafting to* reaction of dopant polymers and driving the formation of the of the brush layer have still to be fully understood. In particular, the effect of molecular weight dispersity on the final composition of the brush layer requires new specific and dedicated experiments to draw a coherent picture of the system. Although we can speculate that the presence of polar terminal-groups plays a key role in producing the observed deviation from the well-assessed mechanism describing the grafting of hydroxy-terminated polymers, a complete comprehension of such a role is still missing. A better understanding of these mechanisms could also shed light on the significant differences observed by modifying the grafting surface like in the case of deglazed and not-deglazed silicon surfaces. It is worth to point out that different substrates could also be characterized by different mechanism of dopant injection into the silicon substrate due to different bonding configuration of P atoms in the dopant source. Accordingly release of the P impurities from the dopant source could determine significant differences in the amount of dopants incorporated into the substrate during the drive-in process. Additionally, different activation efficiencies were observed for dopant atoms diffused from dopant sources formed by grafting the P-terminated polymers on deglazed and not-deglazed surfaces. These results suggest that the initial bonding configuration of the P atoms in the source could play a role in the final bonding configuration of the P atoms within the Si crystal lattice, significantly affecting their activation. In particular, the role of oxygen, nitrogen or carbon contaminants incorporated in the dopant source during the PPD process and diffusing into the silicon substrate during the drive-in process has to be fully elucidated A unified model to explain all the experimental data is currently lacking.

In this respect, by using dopant carriers consisting of monodisperse polypeptoids, part of these problems can be avoided as discussed in the previous chapter. The capability to control in a deterministic way the degree of polymerization of the molecules used as dopant carriers represents a significant breakthrough for this doping technology, moving a step forward in the direction of deterministic doping. However, the research in this direction is only just beginning. Quantitative control over the polymer structure is guaranteed up to 30–40 units, after which the accumulation of small errors during the synthesis becomes no longer negligible implying the loss of control of the effective degree of polymerization of the dopant containing molecules. Consequently, high molecular weights are precluded, limiting the capability to reduce the dose of P atoms into the dopant source below a minimum threshold. In this respect it is worth to note that in the case of high molecular weight polymers the experimental data indicate limited dependence of the grafting density and consequently of the phosphorus dose in the dopant source. Anyway, alternative strategies can be envisioned to control the dopant dose carried onto the substrate by the use of sterically hindered units, but the field is today totally unexplored.

From a more general point of view, the exploitation of the PPD process can be considered officially completed when the technology will be demonstrated to be fully compatible with a process flow for the production of structured microelectronic devices. Recently, PPD method was successfully used to produced doped thin silicon layer in the so called silicon-on-insulator (SOI) morphology. The experimental results demonstrate the effective possibility to control the doping of layers of silicon with thickness $H \geq 5$ nm. Considering that the next generation of gate all around transistors (GAA-FET) are expected to use as channels thin layers ($H \sim 5$ nm), these results suggest that the proposed technology could play a role in the production of the new generations of ultra-scaled transistors [77]. Nevertheless, the upscaling of the proposed PPD approach at the industrial level will require the capability to provide large amounts of phosphorus containing polymers with no variability among the different batches of polymers in order to prevent variability in the performances of the devices due to fluctuations in depth concentration and distribution of dopants. The effective capability to guarantee such a level of reproducibility in the quality of the material represents an extremely demanding challenge from the point of view of the synthesis. On one side conventional polymerization techniques cannot guarantee the required level of control on the molecular weight dispersity of the dopant containing molecule to assure deterministic control on their weight distribution. On the other side the upscaling of the protocols for the synthesis of polypeptoids seems feasible. However, the industrial production of large amounts of polypeptoids on the scale required to fulfil the request of a huge industry like the one of semiconductor devices is anything but trivial. Accordingly, we hope that the reported results will stimulate more work in the field targeting a deeper understanding of the grafting process and the development of advanced synthesis approaches compatible with the upscaling at industrial level.

CRediT authorship contribution statement

Riccardo Chiarcos: Conceptualization, Writing – original draft, Writing – review & editing. **Michele Laus:** Conceptualization, Project

administration, Writing – review & editing. **Michele Perego:** Conceptualization, Project administration, Writing – review & editing.

Declaration of competing interest

The authors declare that they have no known competing financial interests or personal relationships that could have appeared to influence the work reported in this paper.

Data availability

Data will be made available on request.

References

[1] S.M. Sze, K.K. Ng. Physics of Semiconductor Devices, 3Rd ed., John Wiley & Sons, Inc, Hoboken, NJ, USA, 2006 https://doi.org/10.1002/0470068329.
[2] G.E. Moore, Cramming More Components onto Integrated Circuits, Proc. IEEE. 86 (1998) 82–85, https://doi.org/10.1109/JPROC.1998.658762.
[3] T. Skotnicki, G. Merckel, T. Pedron, The Voltage-Doping Transformation: A New Approach to the Modeling of MOSFET Short-Channel Effects, IEEE Electron Device Lett. 9 (1988) 109–112, https://doi.org/10.1109/55.2058.
[4] T. Skotnicki, J.A. Hutchby, T.J. King, H.S.P. Wong, F. Boeuf, The end of CMOS scaling: Toward the introduction of new materials and structural changes to improve MOSFET performance, IEEE Circuits Dev. Mag. 21 (2005) 16–26, https://doi.org/10.1109/MCD.2005.1388765.
[5] J. Ryckaert, R. Baert, D. Verkest, M.H. Na, P. Weckx, D. Jang, P. Schuddinck, B. Chehab, S. Patli, S. Sarkar, O. Zografos, Enabling Sub-5nm CMOS Technology Scaling Thinner and Taller!, in: Tech. Dig. - Int. Electron Devices Meet. IEDM, 2019, p. 8993631, https://doi.org/10.1109/IEDM19573.2019.8993631.
[6] P. Ye, T. Ernst, M.V. Khare, The last silicon transistor: Nanosheet devices could be the final evolutionary step for Moore's Law, IEEE Spectr. 56 (2019) 30–35, https://doi.org/10.1109/MSPEC.2019.8784120.
[7] R. Elbersen, W. Vijselaar, R.M. Tiggelaar, H. Gardeniers, J. Huskens, Fabrication and Doping Methods for Silicon Nano- and Micropillar Arrays for Solar-Cell Applications: A Review, Adv. Mater. 27 (2015) 6781–6796, https://doi.org/10.1002/adma.201502632.
[8] T. Shinada, S. Okamoto, T. Kobayashi, I. Ohdomari, Enhancing semiconductor device performance using ordered dopant arrays, Nature. 437 (2005) 1128–1131, https://doi.org/10.1038/nature04086.
[9] R.W. Keyes, The effect of randomness in the distribution of impurity atoms on FET thresholds, Appl. Phys. 8 (1975) 251–259, https://doi.org/10.1007/BF00896619.
[10] T. Mizuno, J. Okamura, A. Toriumi, Experimental Study of Threshold Voltage Fluctuation Due to Statistical Variation of Channel Dopant Number in MOSFET's, IEEE Trans. Electron Devices. 41 (1994) 2216–2221, https://doi.org/10.1109/16.333844.
[11] H.S.P. Wong, Y. Taur, D.J. Frank, Discrete random dopant distribution effects in nanometer-scale MOSFETs, Microelectron. Reliab. 38 (1998) 1447–1456, https://doi.org/10.1016/s0026-2714(98)00053-5.
[12] P. Ebert, N.D. Jager, K. Urban, E.R. Weber, Nanoscale fluctuations in the distribution of dopant atoms: Dopant-induced dots and roughness of electronic Interfaces, J. Vac. Sci. Technol. B Microelectron. Nanom. Struct. 22 (2004) 2018–2025, https://doi.org/10.1116/1.1771680.
[13] G.C. Tettamanzi, S.J. Hile, M.G. House, M. Fuechsle, S. Rogge, M.Y. Simmons, Probing the Quantum States of a Single Atom Transistor at Microwave Frequencies, ACS Nano. 11 (2017) 2444–2451, https://doi.org/10.1021/acsnano.6b06362.
[14] B.E. Kane, A silicon-based nuclear spin quantum computer, Nature. 393 (1998) 133–137, https://doi.org/10.1038/30156.
[15] S. Kuschlan, R. Chiarcos, M. Laus, F. Pérez-Murano, J. Llobet, M. Fernandez-Regulez, C. Bonafos, M. Perego, G. Seguini, M. De Michielis, G. Tallarida, Periodic Arrays of Dopants in Silicon by Ultralow Energy Implantation of Phosphorus Ions through a Block Copolymer Thin Film, ACS Appl. Mater. Interfaces. 15 (2023) 57928–57940, https://doi.org/10.1021/acsami.3c03782.
[16] M.I. Current, Ion implantation of advanced silicon devices: Past, present and future, Mater. Sci. Semicond. Process. 62 (2017) 13–22, https://doi.org/10.1016/j.mssp.2016.10.045.
[17] P. Rothhardt, C. Demberger, A. Wolf, D. Biro, Co-diffusion from APCVD BSG and POCl3 for industrial n-type solar cells, Energy Procedia. 38 (2013) 305–311, https://doi.org/10.1016/j.egypro.2013.07.282.
[18] E. Garnett, P. Yang, Light trapping in silicon nanowire solar cells, Nano Lett. 10 (2010) 1082–1087, https://doi.org/10.1021/nl100161z.
[19] J. Engelhardt, A. Frey, L. Mahlstaedt, S. Gloger, G. Hahn, B. Terheiden, Boron emitters from doped PECVD layers for n-type crystalline silicon solar cells with LCO, Energy Procedia. 55 (2014) 235–240, https://doi.org/10.1016/j.egypro.2014.08.050.
[20] R. Elbersen, R.M. Tiggelaar, A. Milbrat, G. Mul, H. Gardeniers, J. Huskens, Controlled doping methods for radial p/n junctions in silicon, Adv. Energy Mater. 5 (2015) 1–8, https://doi.org/10.1002/aenm.201401745.
[21] S.H. Baek, B.Y. Noh, I.K. Park, J.H. Kim, Fabrication and characterization of silicon wire solar cells having ZnO nanorod antireflection coating on Al-doped ZnO seed layer, Nanoscale Res. Lett. 7 (2012) 1–8, https://doi.org/10.1186/1556-276X-7-29.
[22] C. Gopalan, P.S. Chakraborty, J. Yang, T. Kim, Z. Wu, M.R. McCartney, S. M. Goodnick, M.N. Kozicki, T.J. Thornton, Shallow source/drain extensions for deep submicron MOSFETs using spin-on-dopants, IEEE Trans. Electron Devices. 50 (2003) 1277–1283, https://doi.org/10.1109/TED.2003.813467.
[23] M.L. Hoarfrost, K. Takei, V. Ho, A. Heitsch, P. Trefonas, A. Javey, R.A. Segalman, Spin-on organic polymer dopants for silicon, J. Phys. Chem. Lett. 4 (2013) 3741–3746, https://doi.org/10.1021/jz4019095.
[24] R. Katsumata, R. Limary, Y. Zhang, B.C. Popere, A.T. Heitsch, M. Li, P. Trefonas, R. A. Segalman, Mussel-Inspired Strategy for Stabilizing Ultrathin Polymer Films and Its Application to Spin-On Doping of Semiconductors, Chem. Mater. 30 (2018) 5285–5292, https://doi.org/10.1021/acs.chemmater.8b02027.
[25] B.C. Popere, B. Russ, A.T. Heitsch, P. Trefonas, R.A. Segalman, Large-Area, Nanometer-Scale Discrete Doping of Semiconductors via Block Copolymer Self-Assembly, Adv. Mater. Interfaces. 2 (2015) 2–7, https://doi.org/10.1002/admi.201500421.
[26] H. Wu, B. Guan, Y. Sun, Y. Zhu, Y. Dan, Controlled doping by self-assembled dendrimer-like macromolecules, Sci. Rep. 7 (2017) 1–10, https://doi.org/10.1038/srep41299.
[27] H. Wu, K. Li, X. Gao, Y. Dan, Phosphorus ionization in silicon doped by self-assembled macromolecular monolayers, AIP Adv. 7 (2017) 1–7, https://doi.org/10.1063/1.4999232.
[28] J.C. Ho, R. Yerushalmi, Z.A. Jacobson, Z. Fan, R.L. Alley, A. Javey, Controlled nanoscale doping of semiconductors via molecular monolayers, Nat. Mater. 7 (2008) 62–67, https://doi.org/10.1038/nmat2058.
[29] M. Susa, K. Kawagishi, N. Tanaka, K. Nagata, Diffusion mechanism of phosphorus from phosphorous vapor in amorphous silicon dioxide film prepared by thermal oxidation, J. Electrochem. Soc. 144 (1997) 2552–2558, https://doi.org/10.1149/1.1837854.
[30] J.C. Ho, R. Yerushalmi, G. Smith, P. Majhi, J. Bennett, J. Halim, V.N. Faifer, A. Javey, Wafer-scale, sub-5 nm junction formation by monolayer doping and conventional spike annealing, Nano Lett. 9 (2009) 725–730, https://doi.org/10.1021/nl8032526.
[31] L. Ye, S.P. Pujari, H. Zuilhof, T. Kudernac, M.P. De Jong, W.G. Van Der Wiel, J. Huskens, Controlling the dopant dose in silicon by mixed-monolayer doping, ACS Appl. Mater. Interfaces. 7 (2015) 3231–3236, https://doi.org/10.1021/am5079368.
[32] W.P. Voorthuijzen, M.D. Yilmaz, W.J.M. Naber, J. Huskens, W.G. Van Der Wiel, Local doping of silicon using nanoimprint lithography and molecular monolayers, Adv. Mater. 23 (2011) 1346–1350, https://doi.org/10.1002/adma.201003625.
[33] B. Long, G. Alessio Verni, J. O'Connell, M. Shayesteh, A. Gangnaik, Y.M. Georgiev, P. Carolan, D. O'Connell, K.J. Kuhn, S.B. Clendenning, R. Nagle, R. Duffy, J. D. Holmes, Doping top-down e-beam fabricated germanium nanowires using molecular monolayers, Mater. Sci. Semicond. Process. 62 (2017) 196–200, https://doi.org/10.1016/j.mssp.2016.10.038.
[34] J. O'Connell, G.A. Verni, A. Gangnaik, M. Shayesteh, B. Long, Y.M. Georgiev, N. Petkov, G.P. McGlacken, M.A. Morris, R. Duffy, J.D. Holmes, Organo-arsenic Molecular Layers on Silicon for High-Density Doping, ACS Appl. Mater. Interfaces. 7 (2015) 15514–15521, https://doi.org/10.1021/acsami.5b03768.
[35] P. Thissen, O. Seitz, Y.J. Chabal, Wet chemical surface functionalization of oxide-free silicon, Prog. Surf. Sci. 87 (2012) 272–290, https://doi.org/10.1016/j.progsurf.2012.10.003.
[36] R.C. Longo, K. Cho, W.G. Schmidt, Y.J. Chabal, P. Thissen, Monolayer doping via phosphonic acid grafting on silicon: Microscopic insight from infrared spectroscopy and density functional theory calculations, Adv. Funct. Mater. 23 (2013) 3471–3477, https://doi.org/10.1002/adfm.201202808.
[37] R. Boukherroub, S. Morin, P. Sharpe, D.D.M. Wayner, Insights into the formation mechanisms of Si-OR monolayers from the thermal reactions of alcohols and aldehydes with SidlD-H, Langmuir. 16 (2000) 7429–7434, https://doi.org/10.1021/la991678z.
[38] D.J. Michalak, S.R. Amy, A. Estève, Y.J. Chabal, Investigation of the chemical purity of silicon surfaces reacted with liquid methanol, J. Phys. Chem. c. 112 (2008) 11907–11919, https://doi.org/10.1021/jp8030539.
[39] J.E. Bateman, R.D. Eagling, B.R. Horrocks, A. Houlton, A deuterium labeling, FTIR, and ab initio investigation of the solution-phase thermal reactions of alcohols and alkenes with hydrogen-terminated silicon surfaces, J. Phys. Chem. b. 104 (2000) 5557–5565, https://doi.org/10.1021/jp000080t.
[40] D.J. Michalak, S. Rivillon, Y.J. Chabal, A. Estève, N.S. Lewis, Infrared spectroscopic investigation of the reaction of hydrogen-terminated, (111)-oriented, silicon surfaces with liquid methanol, J. Phys. Chem. b. 110 (2006) 20426–20434, https://doi.org/10.1021/jp0624303.
[41] E.L. Hanson, J. Schwartz, B. Nickel, N. Koch, M.F. Danisman, Bonding Self-Assembled, Compact Organophosphonate Monolayers to the Native Oxide Surface of Silicon, J. Am. Chem. Soc. 125 (2003) 16074–16080, https://doi.org/10.1021/ja035956z.
[42] A. Vega, P. Thissen, Y.J. Chabal, Environment-controlled tethering by aggregation and growth of phosphonic acid monolayers on silicon oxide, Langmuir. 28 (2012) 8046–8051, https://doi.org/10.1021/la300709n.
[43] B. Bhartia, N. Bacher, S. Jayaraman, S. Khatib, J. Song, S. Guo, C. Troadec, S. R. Puniredd, M.P. Srinivasan, H. Haick, Application of Organophosphonic Acids by One-Step Supercritical CO2 on 1D and 2D Semiconductors: Toward Enhanced Electrical and Sensing Performances, ACS Appl. Mater. Interfaces. 7 (2015) 14885–14895, https://doi.org/10.1021/acsami.5b03597.
[44] R.C. Longo, K. Cho, S. Hohmann, P. Thissen, Mechanism of Phosphorus Transport Through Silicon Oxide during Phosphonic Acid Monolayer Doping, J. Phys. Chem. c. 122 (2018) 10088–10095, https://doi.org/10.1021/acs.jpcc.8b02545.

[45] Y. Shimizu, H. Takamizawa, K. Inoue, F. Yano, Y. Nagai, L. Lamagna, G. Mazzeo, M. Perego, E. Prati, Behavior of phosphorous and contaminants from molecular doping combined with a conventional spike annealing method, Nanoscale. 6 (2014) 706–710, https://doi.org/10.1039/c3nr03605g.

[46] S. Caccamo, R.A. Puglisi, S. Di Franco, L. D'Urso, V. Indelicato, M. Italia, S. Pannitteri, A. La Magna, Silicon doped by molecular doping technique: Role of the surface layers of doped Si on the electrical characteristics, Mater. Sci. Semicond. Process. 42 (2016) 200–203, https://doi.org/10.1016/j.mssp.2015.08.017.

[47] X. Gao, B. Guan, A. Mesli, K. Chen, Y. Dan, Deep level transient spectroscopic investigation of phosphorus-doped silicon by self-assembled molecular monolayers, Nat. Commun. 9 (2018) 1–10, https://doi.org/10.1038/s41467-017-02564-3.

[48] T. Alphazan, L. Mathey, M. Schwarzwälder, T.H. Lin, A.J. Rossini, R. Wischert, V. Enyedi, H. Fontaine, M. Veillerot, A. Lesage, L. Emsley, L. Veyre, F. Martin, C. Thieuleux, C. Copéret, Monolayer Doping of Silicon through Grafting a Tailored Molecular Phosphorus Precursor onto Oxide-Passivated Silicon Surfaces, Chem. Mater. 28 (2016) 3634–3640, https://doi.org/10.1021/acs.chemmater.5b04291.

[49] B. Zdyrko, I. Luzinov, Polymer brushes by the "grafting to" method, Macromol. Rapid Commun. 32 (2011) 859–869, https://doi.org/10.1002/marc.201100162.

[50] W.L. Chen, R. Cordero, H. Tran, C.K. Ober, 50th Anniversary Perspective: Polymer Brushes: Novel Surfaces for Future Materials, Macromolecules. 50 (2017) 4089–4113, https://doi.org/10.1021/acs.macromol.7b00450.

[51] S. Wang, Z. Wang, J. Li, L. Li, W. Hu, Surface-grafting polymers: From chemistry to organic electronics, Mater. Chem. Front. 4 (2020) 692–714, https://doi.org/10.1039/c9qm00450e.

[52] S. Wang, Z. Wang, Y. Huang, Y. Hu, L. Yuan, S. Guo, L. Zheng, M. Chen, C. Yang, Y. Zheng, J. Qi, L. Yu, H. Li, W. Wang, D. Ji, X. Chen, J. Li, L. Li, W. Hu, Directly Patterning Conductive Polymer Electrodes on Organic Semiconductor via in Situ Polymerization in Microchannels for High-Performance Organic Transistors, ACS Appl. Mater. Interfaces. 13 (2021) 17852–17860, https://doi.org/10.1021/acsami.1c01386.

[53] S. Ham, C. Shin, E. Kim, D.Y. Ryu, U. Jeong, T.P. Russell, C.J. Hawker, Microdomain orientation of PS-b-PMMA by controlled interfacial interactions, Macromolecules. 41 (2008) 6431–6437, https://doi.org/10.1021/ma8007338.

[54] E. Han, K.O. Stuen, Y.H. La, P.F. Nealey, P. Gopalan, Effect of composition of substrate-modifying random copolymers on the orientation of symmetric and asymmetric diblock copolymer domains, Macromolecules. 41 (2008) 9090–9097, https://doi.org/10.1021/ma8018393.

[55] E. Han, K.O. Stuen, M. Leolukman, C.C. Liu, P.F. Nealey, P. Gopalan, Perpendicular orientation of domains in cylinder-forming block copolymer thick films by controlled interfacial interactions, Macromolecules. 42 (2009) 4896–4901, https://doi.org/10.1021/ma9002903.

[56] F. Ferrarese Lupi, T.J. Giammaria, F.G. Volpe, F. Lotto, G. Seguini, B. Pivac, M. Laus, M. Perego, High aspect ratio PS-b-PMMA block copolymer masks for lithographic applications, ACS Appl, Mater. Interfaces. 6 (2014) 21389–21396, https://doi.org/10.1021/am506391n.

[57] F. Ferrarese Lupi, I. Murataj, F. Celegato, A. Angelini, F. Frascella, R. Chiarcos, D. Antonioli, V. Gianotti, P. Tiberto, C.F. Pirri, L. Boarino, M. Laus, Tailored and Guided Dewetting of Block Copolymer/Homopolymer Blends, Macromolecules. 53 (2020) 7207–7217, https://doi.org/10.1021/acs.macromol.0c01126.

[58] K. Sparnacci, D. Antonioli, V. Gianotti, M. Laus, F. Ferrarese Lupi, T.J. Giammaria, G. Seguini, M. Perego, Ultrathin Random Copolymer-Grafted Layers for Block Copolymer Self-Assembly, ACS Appl, Mater. Interfaces. 7 (2015) 10944–10951, https://doi.org/10.1021/acsami.5b02201.

[59] M. Perego, G. Seguini, E. Arduca, A. Nomellini, K. Sparnacci, D. Antonioli, V. Gianotti, M. Laus, Control of Doping Level in Semiconductors via Self-Limited Grafting of Phosphorus End-Terminated Polymers, ACS Nano. 12 (2018) 178–186, https://doi.org/10.1021/acsnano.7b05459.

[60] I. Luzinov, D. Julthongpiput, H. Malz, J. Pionteck, V.V. Tsukruk, Polystyrene layers grafted to epoxy-modified silicon surfaces, Macromolecules. 33 (2000) 1043–1048, https://doi.org/10.1021/ma990926v.

[61] K.S. Iyer, B. Zdyrko, H. Malz, J. Pionteck, I. Luzinov, Polystyrene layers grafted to macromolecular anchoring layer, Macromolecules. 36 (2003) 6519–6526, https://doi.org/10.1021/ma034460z.

[62] L.J. Norton, V. Smigolova, M.U. Pralle, A. Hubenko, K.H. Dai, E.J. Kramer, S. Hahn, C. Berglund, B. DeKoven, Effect of End-Anchored Chains on the Adhesion at a Thermoset-Thermoplastic Interface, Macromolecules. 28 (1995) 1999–2008, https://doi.org/10.1021/ma00110a038.

[63] E.J. Kramer, Grafting Kinetics of End-Functional Polymers at Melt Interfaces, Isr. J. Chem. 35 (1995) 49–54, https://doi.org/10.1002/ijch.199500010.

[64] X. Zhao, W. Zhao, X. Zheng, M.H. Rafailovich, J. Sokolov, S.A. Schwarz, M.A. A. Pudensi, T.P. Russell, S.K. Kumar, L.J. Fetters, Configuration of grafted polystyrene chains in the melt: Temperature and concentration dependence, Phys. Rev. Lett. 69 (1992) 776–779, https://doi.org/10.1103/PhysRevLett.69.776.

[65] B.J. Kim, G.H. Fredrickson, E.J. Kramer, Analysis of reaction kinetics of end-functionalized polymers at a PS/P2VP interface by DSIMS, Macromolecules. 40 (2007) 3686–3694, https://doi.org/10.1021/ma0611218.

[66] R.A.L. Jones, L.J. Norton, K.R. Shull, E.J. Kramer, G.P. Felcher, A. Karim, L. J. Fetters, Interfacial Segment Density Profiles of End-Anchored Polymers in a Melt, Macromolecules. 25 (1992) 2359–2368, https://doi.org/10.1021/ma00035a012.

[67] M. Laus, R. Chiarcos, V. Gianotti, D. Antonioli, K. Sparnacci, G. Munaò, G. Milano, A. De Nicola, M. Perego, Evidence of Mechanochemical Control in "grafting to" Reactions of Hydroxy-Terminated Statistical Copolymers, Macromolecules. 54 (2021) 499–508, https://doi.org/10.1021/acs.macromol.0c02142.

[68] R. Chiarcos, M. Perego, M. Laus, Polymer Brushes by Grafting to Reaction in Melt: New Insights into the Mechanism, Macromol. Chem. Phys. 224 (2023) 1–17, https://doi.org/10.1002/macp.202200400.

[69] T.J. Giammaria, F. Ferrarese Lupi, G. Seguini, K. Sparnacci, D. Antonioli, V. Gianotti, M. Laus, M. Perego, Effect of Entrapped Solvent on the Evolution of Lateral Order in Self-Assembled P(S-r-MMA)/PS-b-PMMA Systems with Different Thicknesses, ACS Appl, Mater. Interfaces. 9 (2017) 31215–31223, https://doi.org/10.1021/acsami.6b14332.

[70] K. Sparnacci, R. Chiarcos, V. Gianotti, M. Laus, T.J. Giammaria, M. Perego, G. Munaò, G. Milano, A. De Nicola, M. Haese, L.P. Kreuzer, T. Widmann, P. Müller-Buschbaum, Effect of Trapped Solvent on the Interface between PS-b-PMMA Thin Films and P(S-r-MMA) Brush Layers, ACS Appl. Mater. Interfaces. 12 (2020) 7777–7787, https://doi.org/10.1021/acsami.9b20801.

[71] T.J. Giammaria, M. Laus, R. Chiarcos, C.K. Ober, G. Seguini, M. Perego, Influence of spin casting solvent on the self-assembly of silicon-containing block copolymer thin films via high temperature thermal treatment, Polym. Int. 71 (2022) 426–435, https://doi.org/10.1002/pi.6362.

[72] R.A.L. Jones, R.J. Lehnert, H. Schönherr, J. Vancso, Factors affecting the preparation of permanently end-grafted polystyrene layers, Polymer (guildf). 40 (1999) 525–530, https://doi.org/10.1016/S0032-3861(98)00249-3.

[73] F.F. Lupi, T.J. Giammaria, G. Seguini, M. Ceresoli, M. Perego, D. Antonioli, V. Gianotti, K. Sparnacci, M. Laus, Flash grafting of functional random copolymers for surface neutralization, J. Mater. Chem. c. 2 (2014) 4909–4917, https://doi.org/10.1039/c4tc00328d.

[74] M. Perego, F. Caruso, G. Seguini, E. Arduca, R. Mantovan, K. Sparnacci, M. Laus, Doping of silicon by phosphorus end-terminated polymers: Drive-in and activation of dopants, J. Mater. Chem. c. 8 (2020) 10229–10237, https://doi.org/10.1039/d0tc01856b.

[75] P.P. Altermatt, A. Schenk, G. Heiser, A simulation model for the density of states and for incomplete ionization in crystalline silicon. I. Establishing the model in Si: P, J. Appl. Phys. 100 (2006) 1–10, https://doi.org/10.1063/1.2386934.

[76] G. Barin, G. Seguini, R. Chiarcos, V.M. Ospina, M. Laus, C. Lenardi, M. Perego, Phosphorus activation in silicon: To deglaze or not to deglaze, that is the question, Mater. Sci. Semicond. Process. 165 (2023) 107691, https://doi.org/10.1016/j.mssp.2023.107691.

[77] A. Pulici, S. Kuschlan, G. Seguini, F. Taglietti, M. Fanciulli, R. Chiarcos, M. Laus, M. Perego, Electrical characterization of thin silicon-on-insulator films doped by means of phosphorus end-terminated polymers, Mater. Sci. Semicond. Process. 163 (2023) 107548, https://doi.org/10.1016/j.mssp.2023.107548.

[78] S.S. Li, W.R. Thurber, The dopant density and temperature dependence of electron mobility and resistivity in n-type silicon, Solid. State Electron. 20 (1977) 609–616, https://doi.org/10.1016/0038-1101(77)90100-9.

[79] R. Chiarcos, V. Gianotti, M. Cossi, A. Zoccante, D. Antonioli, K. Sparnacci, M. Laus, F.E. Caligiore, M. Perego, Thermal Degradation in Ultrathin Films Outperforms Dose Control of n-Type Polymeric Dopants for Silicon, ACS Appl. Electron. Mater. 1 (2019) 1807–1816, https://doi.org/10.1021/acsaelm.9b00364.

[80] S. Grimaldi, J.P. Finet, F. Le Moigne, A. Zeghdaoui, P. Tordo, D. Benoit, M. Fontanille, Y. Gnanou, Acyclic β-phosphonylated nitroxides: a new series of counter-radicals for "living"/controlled free radical polymerization, Macromolecules. 33 (2000) 1141–1147, https://doi.org/10.1021/ma9913414.

[81] K. Sparnacci, D. Antonioli, V. Gianotti, M. Laus, G. Zuccheri, F. Ferrarese Lupi, T. J. Giammaria, G. Seguini, M. Ceresoli, M. Perego, Thermal stability of functional P (S-r-MMA) random copolymers for nanolithographic applications, ACS Appl, Mater. Interfaces. 7 (2015) 3920–3930, https://doi.org/10.1021/am509088s.

[82] L. Michalek, K. Mundsinger, L. Barner, C. Barner-kowollik, Quantifying Solvent Effects on Polymer Surface Grafting, ACS Appl. Polym. Mater. 8 (2019) 800–805, https://doi.org/10.1021/acsmacrolett.9b00336.

[83] L. Michalek, K. Mundsinger, C. Barner-Kowollik, L. Barner, The long and the short of polymer grafting, Polym. Chem. 10 (2019) 54–59, https://doi.org/10.1039/c8py01470a.

[84] D. Antonioli, R. Chiarcos, V. Gianotti, M. Terragno, M. Laus, G. Munaò, G. Milano, A. De Nicola, M. Perego, Inside the brush: Partition by molecular weight in grafting to reactions from melt, Polym. Chem. 12 (2021) 6538–6547, https://doi.org/10.1039/d1py01303c.

[85] R. Chiarcos, D. Antonioli, V. Gianotti, M. Laus, G. Munaò, G. Milano, A. De Nicola, M. Perego, Short vs. long chains competition during "grafting to" process from melt, Polym. Chem. 13 (2022) 3904–3914, https://doi.org/10.1039/d2py00364c.

[86] R. Chiarcos, D. Antonioli, V. Ospina, M. Laus, M. Perego, V. Gianotti, Quantification of molecular weight discrimination grafting to reactions from ultrathin polymer films by matrix-assisted laser desorption/ionization time-of-flight mass spectrometry, Analyst. 146 (2021) 6145–6155, https://doi.org/10.1039/d1an01329g.

[87] M. Perego, S. Kuschlan, G. Seguini, R. Chiarcos, V. Gianotti, D. Antonioli, K. Sparnacci, M. Laus, Silicon Doping by Polymer Grafting: Size Distribution Matters, ACS Appl. Polym. Mater. 3 (2021) 6383–6393, https://doi.org/10.1021/acsapm.1c01157.

[88] V. Kottisch, D.T. Gentekos, B.P. Fors, "Shaping" the Future of Molecular Weight Distributions in Anionic Polymerization, ACS Macro Lett. 5 (2016) 796–800, https://doi.org/10.1021/acsmacrolett.6b00392.

[89] D.T. Gentekos, L.N. Dupuis, B.P. Fors, Beyond Dispersity: Deterministic Control of Polymer Molecular Weight Distribution, J. Am. Chem. Soc. 138 (2016) 1848–1851, https://doi.org/10.1021/jacs.5b13565.

[90] D.T. Gentekos, J. Jia, E.S. Tirado, K.P. Barteau, D.M. Smilgies, R.A. Distasio, B. P. Fors, Exploiting Molecular Weight Distribution Shape to Tune Domain Spacing in Block Copolymer Thin Films, J. Am. Chem. Soc. 140 (2018) 4639–4648, https://doi.org/10.1021/jacs.8b00694.

[91] R. Whitfield, K. Parkatzidis, N.P. Truong, T. Junkers, A. Anastasaki, Tailoring Polymer Dispersity by RAFT Polymerization: A Versatile Approach, Chem. 6 (2020) 1340–1352, https://doi.org/10.1016/j.chempr.2020.04.020.

[92] R. Whitfield, K. Parkatzidis, M. Rolland, N.P. Truong, A. Anastasaki, Tuning Dispersity by Photoinduced Atom Transfer Radical Polymerisation: Monomodal Distributions with ppm Copper Concentration, Angew. Chemie - Int. Ed. 58 (2019) 13323–13328, https://doi.org/10.1002/anie.201906471.

[93] R. Whitfield, N.P. Truong, D. Messmer, K. Parkatzidis, M. Rolland, A. Anastasaki, Tailoring polymer dispersity and shape of molecular weight distributions: methods and applications, Chem. Sci. 10 (2019) 8724–8734, https://doi.org/10.1039/c9sc03546j.

[94] R.B. Merrifield, Solid phase peptide synthesis. I. The synthesis of a Tetrapeptide, J. Am. Chem. Soc. 85 (1963) 2149–2154, https://doi.org/10.1021/ja00897a025.

[95] R.N. Zuckermann, J.M. Kerr, S.B.H. Kent, W.H. Moos, Efficient Method for the Preparation of Peptoids [Oligo(N-substituted glycines)] by Submonomer Solid-Phase Synthesis, J. Am. Chem. Soc. 114 (1992) 10646–10647, https://doi.org/10.1021/ja00052a076.

[96] N. Gangloff, J. Ulbricht, T. Lorson, H. Schlaad, R. Luxenhofer, Peptoids and Polypeptoids at the Frontier of Supra- and Macromolecular Engineering, Chem. Rev. 116 (2016) 1753–1802, https://doi.org/10.1021/acs.chemrev.5b00201.

[97] V.M. Ospina, R. Chiarcos, D. Antonioli, V. Gianotti, M. Laus, S. Kuschlan, C. Wiemer, M. Perego, Brush Layers of Bioinspired Polypeptoids for Deterministic Doping of Semiconductors, ACS Appl. Electron. Mater. 4 (2022) 6029–6037, https://doi.org/10.1021/acsaelm.2c01182.